# Nucleophilic Vinylic Substitution. A Theoretical Study

Drora Cohen,[†] Rony Bar,[†] and Sason S. Shaik*[‡§]

*Contribution from the Department of Chemistry, Bar Ilan University, Ramat Gan,
52100 Israel, and Laboratoire de Chimie Théorique,[⊥] Université de Paris Sud, 91405 Orsay,
France. Received November 14, 1984. Revised Manuscript Received May 18, 1985*

Abstract: Reactivity trends in nucleophilic vinylic substitutions are discussed in a two-pronged approach. Ab initio computations of eight reactions are performed. The results of transition-state geometries, reaction barriers, and mechanistic variety are used in conjunction with experimental evidence as the data stock to be patterned. The state correlation diagram is utilized for this last purpose. Potential energy profiles are constructed and the origin of barriers is projected. Expected patterns are predicted and compared with the computed and experimental data in the following areas: (a) the spectrum of mechanism, stepwise, and single-step reactions; (b) trends in reaction barriers and "intrinsic barriers" for attack and leaving-group expulsion steps; (c) trends in transition-state geometries and the role of geometric distortions.

Nucleophilic vinylic substitution (NVS) is rich in mechanistic and reactivity information. From an experimental mechanistic angle there exsits overwhelming evidence[1] for a spectrum that involves addition and elimination type steps as shown in eq 1. In

$$XRC = CR'R'' + N:^- \xrightarrow{a} (XNRC—\ddot{C}R'R'')^- \xrightarrow{b}$$
$$NRC=CR'R'' + X:^- \quad (1)$$
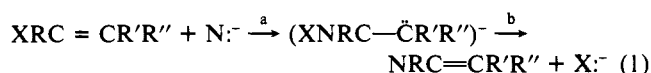
some reactions carbanion formation (step a) is rate controlling, while in others, leaving-group (X) expulsion is the slow step.[1] Still in other reactions—though in very few—the steps seem to merge into a single phase.[2]

In this entire mechanistic spectrum retention of the isomeric identity of the olefin is the preponderant stereochemical outcome of the substitution. This evidence has been recently patterned by Rappoport[1b] in terms of the variable transition-state concept.

The experimental reactivity data, on the addition step, pose some interesting problems. While general trends such as the superior reactivity of powerful over poor acceptor olefins[1a,b] follow simple FMO arguments, there exist also some opposing trends. For example, fluoro olfeins are poorer electron acceptors (have higher π^*-LUMO) than ethylene.[3] But nevertheless fluoroethylenes react many orders of magnitude faster than ethylene.[1f,4] Similarly tetrafluoroethylene seems to react faster than tetrachloroethylene,[1f] despite the fact that the π^*-LUMO of the latter is 2.7 eV lower in energy.[3b,c] Other powerful acceptor olefins like nitrostyrene, benzylidene Meldrum's acid, etc., have been reported by Bernasconi and co-workers[5] to possess higher "intrinsic barriers" for attack relative to less powerful acceptors.

Some of these reactivity trends seem to better follow the Bell–Evans–Polanyi (BEP) principle,[6] which states that increased exothermicity leads to a rate increase. For example, Park's reactivity rule,[1a,f,g,7] that nucleophilic attack will assume the course that leads to the most stable carbanion, works well for olefins that lead to α-chloro vs. α-fluoro carbanions (see also Bach and Wolber[8a]). However, other trends of similar chemical nature defy the BEP principle. Notable among these latter trends is the important mechanistic tool, the "element effect"[9] ($k_F > k_{Cl}$). Thus fluoro olefins react faster than chloro olefins at the halo-substituted carbon in **1**, despite the superior exothermicity of the chloro olefin

$$R'R''C = \underset{\displaystyle \uparrow}{C}RX \qquad k_{X=F} > k_{X=Cl}$$

1
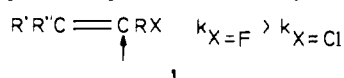
reaction and the lower π^*-LUMO of chloro olefins[3] (see computational results in Table II and ref 8a). Other trends of this kind have been reported by Bernasconi and co-workers,[5a,e] who

have found that delocalized nucleophiles (e.g., $(NC)_2CH^-$), which lead to highly exothermic reactions, have higher "intrinsic barriers" than do less powerful donor nucleophiles whose reactions are less exothermic.

Leaving-group expulsion rates[10] pose generally the same types of problems as does the attack phase (step b vs. a, eq 1). One of the interesting examples is the higher barrier[5e] for expulsion of X^-: = $NO_2CH_2^-$ relative to $X:^-$ = $NCCH_2^-$—which is in contrast to both FMO arguments and the BEP principle and which suggests[5d] that resonance-stabilized $X:^-$ leaving groups tend to have higher "intrinsic barriers" than less stabilized and charge-localized $X:^-$ leaving groups.

From a theoretical angle there have appeared a few investigations[8,11,12] that have treated various aspects of the reaction mechanism. Thus, the factors controlling the stereochemical outcome of the reaction (eq 1) seem to be well understood in terms of the hyperconjugative preferences of the carbanion, as described

(1) (a) Rappoport, Z. *Adv. Phys. Org. Chem.* **1969**, *7*, 1. (b) Rappoport, Z. *Acc. Chem. Res.* **1981**, *14*, 7. (c) Modena, G. *Acc. Chem. Res.* **1971**, *4*, 73. (d) Miller, S. I. *Tetrahedron* **1977**, *33*, 1211. (e) Chambers, R. D.; Mobes, R. H. In "Advances in Fluorine Chemistry"; Stacey, M.; Tatlow, J. C.; Sharp, A. G., Eds.; Butterworth: London, 1965; p 50. (f) Chambers, R. D. "Fluorine in Organic Chemistry"; Interscience: London, 1973; p 148–170, 104–106. (g) Park, D. J.; McMurtry, R. J.; Adams, J. H. *Fluorine Chem. Rev.* **1968**, *2*, 55.

(2) (a) Dodd, D.; Johnson, M. D.; Meeks, B. S.; Titchmarsh, D. M.; Doung, K. N. V.; Gaudemer, A. *J. Chem. Soc., Perkin Trans. 2* **1976**, 1261. (b) Maffeo, C. V.; Marchese, G.; Naso, F.; Ronzini, L. *J. Chem. Soc., Perkin Trans. 1* **1979**, 92.

(3) (a) Chiu, N. S.; Burrow, P. D.; Jordan, K. D. *Chem. Phys. Lett.* **1979**, *68*, 121. (b) Burrow, P. D.; Modelli, A.; Chiu, N. S.; Jordan, K. D. *Chem. Phys. Lett.* **1981**, *82*, 270. (c) Kaufel, R.; Illenberger, E.; Baumgärtel, H. *Chem. Phys. Lett.* **1984**, *106*, 342.

(4) Evans, C. M.; Kirby, A. J. *J. Am. Chem. Soc.* **1982**, *104*, 4705.

(5) Rates for attack and explusion steps appear in: (a) Bernasconi, C. F.; Zitomer, J. L.; Fox, J. P.; Howard, K. A. *J. Org. Chem.* **1984**, *49*, 482. (b) Bernasconi, C. F.; Murray, C. J.; Fox, J. P.; Carré, D. J. *J. Am. Chem. Soc.* **1983**, *105*, 4349. (c) Bernasconi, C. F.; Murray, C. J. *J. Am. Chem. Soc.* **1984**, *106*, 3257. (d) Bernasconi, C. F. *Pure Appl. Chem.* **1982**, *54*, 2335. (e) Bernasconi, C. F.; Howard, K. A.; Kanavrioti, A. *J. Am. Chem. Soc.* **1984**, *106*, 6827.

(6) (a) Bell, R. P. *Proc. R. Soc. London A* **1936**, *154*, 414. (b) Evans, M. G.; Polanyi, M. *Trans. Faraday Soc.* **1938**, *34*, 49. *Ibid.* **1937**, *33*, 448. *Ibid.* **1935**, *31*, 875. *Ibid.* **1938**, *34*, 11. *Ibid.* **1936**, *32*, 1333.

(7) Park, J. D.; Lacher, J. R.; Dick, J. R. *J. Org. Chem.* **1966**, *31*, 1116.

(8) (a) Bach, R. D.; Wolber, G. J. *J. Am. Chem. Soc.* **1984**, *106*, 1401. (b) Bach, R. D.; Badger, R. C.; Lang, T. J. *J. Am. Chem. Soc.* **1979**, *101*, 2845.

(9) Bunnett, J. F.; Garbisch, E. W., Jr.; Pruitt, K. M. *J. Am. Chem. Soc.* **1957**, *79*, 385.

(10) For a review on leaving-group expulsions see: Stirling, C. J. M. *Acc. Chem. Res.* **1979**, *12*, 198.

(11) (a) Apeloig, Y.; Rappoport, Z. *J. Am. Chem. Soc.* **1979**, *101*, 5095. (b) Texier, F.; Henri-Rousseau, O.; Bourgois, J. *Bull. Soc. Chim. Fr.* **1979**, *86*. (c) Stohrer, W. D. *Tetrahedron Lett.* **1975**, 207.

(12) (a) Strozier, R. W.; Caramella, P.; Houk, K. N. *J. Am. Chem. Soc.* **1979**, *101*, 134. (b) Houk, K. N.; Strozier, R. W.; Rozeboom, M. D.; Nagase, S. *J. Am. Chem. Soc.* **1982**, *104*, 323. (c) Houk, K. N. *Top. Curr. Chem.* **1979**, *79*, 1.

† Bar Ilan University.
‡ Université de Paris Sud.
§ Permanent address: Department of Chemistry, Ben-Gurion University, Beer Sheva 84105, Israel.
⊥ The Laboratoire de Chimie Théorique is associated with the CNRS, UA 506.

232 *J. Am. Chem. Soc.. Vol. 108, No. 2, 1986*

Cohen et al.

Table I. Summary of Features of Reactions 1–8

reacn	E_{AT}^{*a}	E_{El}^{*b}	mechanistic qualities
(1) $H^{*-} + H_2C{=}CH_2 \rightarrow H_2C{=}CH^*H + H^-$	12.65	25.2	stepwise
(2) $H^{*-} + H_2C{=}CHF \rightarrow H_2C{=}CH^*H + F^-$	6.93	$>0^c$	two steps, A_1 does not exist
(3) $H^{*-} + H_2C{=}CHF \rightarrow H^*HC{=}CHF + H^-$	9.90	66.1	stepwise
(4) $H^{*-} + H_2C{=}CF_2 \rightarrow H^*HC{=}CF_2 + H^-$	6.76	60.6	stepwise
(5) $H^{*-} + H_2C{=}CF_2 \rightarrow H_2C{=}CH^*F + F^-$	$<0^d$	0.8	stepwise
(6) $H^{*-} + FHC{=}CHF \rightarrow HFC{=}CH^*H + F^-$	2.69	0.3	stepwise
(7) $H^{*-} + H_2C{=}CHCl \rightarrow H_2C{=}CH^*H + Cl^-$	7.91	$<0^e$	single step
(8) $H^{*-} + H_2C{=}CHCl \rightarrow H^*HC{=}CHCl + H^-$	0.52	59.9	stepwise

^{a}DZ//4-31G results (kcal/mol). ^{b}4-31G//4-31G results (kcal/mol). ^{c}A small barrier exists with the 3-21G and 6-31G* bases. ^{d}No TS; energy decreases monotonically toward A_1. ^{e}Energy decreases monotonically from the TS toward $H_2C{=}CH_2 + Cl^-$ (with the 4-31G and 3-21G bases).

by Apeloig and Rappoport,[11a] Rousseau and co-workers,[11b] Stohrer,[11c] and Miller.[1d] The trajectory of nucleophilic attacks, the role of geometric distortions, and the failure of *simplified* FMO arguments to account for reactivity trends have been discussed by Houk and co-workers,[12] while the role of HOMO–HOMO interactions has been projected by Bach and Wolber.[8a]

Though a great deal of understanding has been achieved and explanations have been offered for many of the above problems, there seems to be missing a theoretical approach that enables the entire reaction profile to be constructed. Our aim in this paper is to utilize the state correlation diagram approach[13,14] to generate the reaction profile and, thereby, to derive simple expressions for the various barriers, to understand the factors that control the structure of the transition state, and to outline the conditions for occurrence of single-step and stepwise reactions.

The strategy is two-pronged: a computational study of a few NVS reactions will provide a stock of information and will be followed by the development of the model.[13,14] The insight provided by the model will be then utilized to pattern the various aspects of the computational data and relate it to experimental evidence.

Computational Methods

All calculations used the GAUSSIAN 80 package of programs.[15] The geometries were fully optimized with the split-valence 4-31G basis set[16] using analytical energy gradients.[17] Energy minima and transition states were rigorously located by diagonalizing the matrix of force constants.[18] In two instances that are specified later on, the 3-21G and 6-31G* bases[19] were used too.

The 4-31G geometries were then used for single-point calculations with an extended double-ζ (DZ) basis set. This extended basis set involves Dunning-contracted[20] functions of Huzinaga's atomic orbitals[21] (9s5p/4s and 11s7p/4s with hydrogen atom scaled[21] by 1.2). These basis functions were augmented with a single d-type Gaussian on the heavy atoms[20,22] (with function exponents: C, 0.75; F, 0.90; for Cl, see ref 22) and a p-type function on the hydrogens[20] (exponent 0.75). For a more accurate

Table II. Computed (DZ//4-31G) Barriers (E_{AT}^*) and Reaction Energies (ΔE_{AT}) for the Attack Phase of Nucleophilic Substitution Reactions
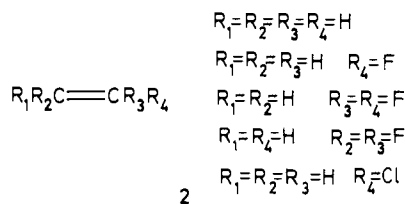
reacn	$E_{AT}^{*a,b}$	ΔE_{AT}^a	A_0^{π}, eV
(1) $H^- + H_2C{=}CH_2 \rightarrow H_3CCH_2^-$	12.65	−16.03	−1.80
(2) $H^- + HFC{=}CH_2 \rightarrow H_2FCH_2^-$	6.93	-29.55^d	−1.91
(3) $H^- + H_2C{=}CHF \rightarrow H_3CCHF^-$	9.90	−27.33	−1.91
(4) $H^- + H_2C{=}CF_2 \rightarrow H_3CCF_2^-$	6.76	−47.31	−2.39
(5) $H^- + F_2C{=}CH_2 \rightarrow HF_2CCH_2^-$	$<0^c$	−46.77	−2.39
(6) $H^- + c\text{-}FHC{=}CHF \rightarrow H_2FCCHF^-$	2.69	−46.13	−2.18
(7) $H^- + HClC{=}CH_2 \rightarrow \text{"}H_2ClCCH_2^{-\text{"}}$	7.91	e	−1.28
(8) $H^- + H_2C{=}CHCl \rightarrow H_3CCHCl^-$	0.52	−47.60	−1.28

^{a}In kcal/mol. $^bE_{AT}^* = E(\text{TS}) - E(\text{R})$. See 3 in the text. The 4-31G//4-31G results exhibit an identical trend, but E_{AT}^* is generally negative. $\Delta E_{AT} = E(A_1) - E(\text{R})$. ^{c}No transition state is observed. Energy descends smoothly towards the carbanion. ^{d}DZ//3-21G result. 4-31G leads to decomposition of $FCH_2CH_2^-$. ^{e}No carbanion exists. $\Delta E = -106.72$ kcal/mol for $H^- + H_2C{=}CHCl \rightarrow Cl^- + H_2C{=}CH_2$.

description of the anionic species, the valence parts of the basis sets were augmented by diffuse p-type functions on the heavy atoms[20,23] (exponents: C, 0.0365; F, 0.0796; Cl, 0.0490) and a diffuse s-type function on the hydrogens[24] (the exponent, 0.0444, was selected as one-half of the smallest atomic orbital exponent). The final DZ basis sets that were used in this study are then as follows: [2s1p] + [1s] for H, [3s2p1d] + [1p] for F and C, and [6s4p1d] + [1p] for Cl.

The energies of the various species are collected in the supplementary material and are denoted by DZ//4-31G—which means single-point calculations with the DZ basis set at the 4-31G optimized geometry. In what follows, the energetics of the reactions studied are always referred to as DZ//4-31G unless noted otherwise.

Description of the Computational Results. The computational studies involve eight nucleophilic reactions of H^- with the five different olefins shown in 2. The choice of the olefins was made

$$R_1R_2C{=\!=}CR_3R_4$$

$$\begin{aligned}&R_1{=}R_2{=}R_3{=}R_4{=}H\\&R_1{=}R_2{=}R_3{=}H \quad R_4{=}F\\&R_1{=}R_2{=}H \quad R_3{=}R_4{=}F\\&R_1{=}R_4{=}H \quad R_2{=}R_3{=}F\\&R_1{=}R_2{=}R_3{=}H \quad R_4{=}Cl\end{aligned}$$

2

so as to cover the range of problems that are mentioned in the introduction.

The various computed quantities are specified hereafter by the designators shown in the reaction sequence in 3, and a summary of reactivity features is given in Table I. Only one reaction (no. 7: $H^- + H_2C{=}CHCl \rightarrow H_2C{=}CH_2 + Cl^-$) is seen to follow a single-step mechanism. The rest of the reactions follow a stepwise mechanism via either the carbanion intermediate A_2 (reaction 2) or both A_1 and A_2 intermediates (reactions 1, 3–6, and 8).

(13) Shaik, S. S. *J. Am. Chem. Soc.* **1981**, *103*, 3692.

(14) (a) Shaik, S. S. *Nouv. J. Chim.* **1982**, *6*, 159. (b) *Ibid.* **1983**, *7*, 201. (c) Shaik, S. S.; Pross, A. *J. Am. Chem. Soc.* **1982**, *104*, 2708. (d) Shaik, S. S. *J. Am. Chem. Soc.* **1983**, *105*, 4359. (e) Shaik, S. S. *J. Am. Chem. Soc.* **1984**, *106*, 1227. (f) Pross, A.; Shaik, S. S. *Acc. Chem. Res.* **1983**, *16*, 363. (g) Shaik, S. S. *Prog. Phys. Org. Chem.* **1985**, *15*, 0000.

(15) Binkley, J. B.; Whitside, R. A.; Krishnan, R.; Seeger, R.; Defrees, D. J.; Schlegel, H. B.; Topiol, S.; Kahn, L. K.; Pople, J. A. GAUSSIAN 80, Carnegie-Mellon University, 1980.

(16) Ditchfield, R.; Hehre, W. J.; Pople, J. A. *J. Chem. Phys.* **1971**, *54*, 724.

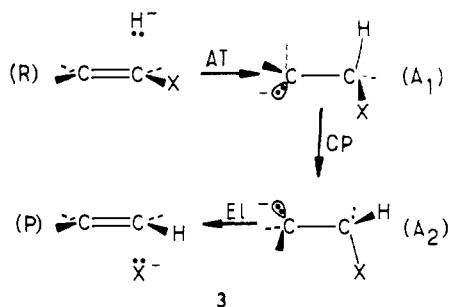(17) Schlegel, H. B.; Wolfe, S.; Bernardi, F. *J. Chem. Phys.* **1975**, *63*, 3632.

(18) Pople, J. A.; Krishnan, R.; Schlegel, H. B.; Binkley, J. S. *Int. J. Quantum Chem.* **1979**, *S13*, 225.

(19) (a) Binkley, J. S.; Pople, J. A.; Hehre, W. J. *J. Am. Chem. Soc.* **1980**, *102*, 939. (b) Hariharan, P. C.; Pople, J. A. *Theor. Chim. Acta* **1973**, *23*, 208; *Chem. Phys. Lett.* **1972**, *16*, 217.

(20) (a) Dunning, T. H., Jr.; Hay, P. J. In "Modern Theoretical Chemistry"; Schaefer, H. F., III, Ed.; Plenum Press: New York, 1977; Vol. 3, pp 22–25. (b) Dunning, T. H., Jr. *J. Chem. Phys.* **1970**, *53*, 2823.

(21) Huzinaga, S. *J. Chem. Phys.* **1965**, *42*, 1293. The primitive bases correspond to C,F (9s5p), Cl (11s7p), and H (4s).

(22) d-Type functions for Cl were taken from Roos, B.; Siegbahn, P. *Theor. Chim. Acta* **1970**, *17*, 199.

(23) The diffuse p functions for C and F were obtained with the even-tempered criterion in: Raffenetti, R. C. *J. Chem. Phys.* **1973**, *59*, 5936.

(24) The importance of diffuse functions for energetics involving anionic species is demonstrated in: Clark, T.; Chandresekhar, J.; Spitznagel, G. W.; Schleyer, P. v. R. *J. Comput. Chem.* **1983**, *4*, 294. Spitznagel, G. W.; Clark, T.; Chandresekhar, J.; Schleyer, P. v. R. *Ibid.* **1982**, *3*, 363.

3

Reaction Barriers and Transition-State Structures for the Attack Phase. Reaction barriers ($E_{AT}{}^*$) and reaction energies (ΔE_{AT}) for the attack step are collected in Table II along with the vertical electron affinities of the reacting olefins ($A_0{}^\pi$).[3] The trends in the barriers correlate with what is known experimentally from solution data. The relative reactivity of ethylene to fluoro- and chloroethylene (entry 1 vs. 2–8) and the superior reactivity of 1,1-difluoroethylene at CF_2 (entry 5) are in accord with experimental data.[1a,b,g,25] Similarly, the regiochemical preferences of attack, on the F-substituted carbons in $H_2C{=}CHF$ and $H_2C{=}CF_2$ (entries 2 vs. 3; 4 vs. 5) and away from the Cl-substituted carbon in $H_2C{=}CHCl$ (entry 7 vs. 8), are also in line with the experimental data.[1b,f,g,26]

The experimentally observed[1] "element effect", $k_F > k_{Cl}$ is also reproduced by the computational study (entries 2 vs. 7). And finally Park's rule[7] that reactions leading to α-Cl carbanions will be faster than those that lead to α-F carbanions is also manifested in the theoretical results (entries 8 vs. 3).

The reactivity problems that are provided by the set can be identified by inspecting the $A_0{}^\pi$ values (which vary as do the corresponding π^*-LUMO levels[3]) and the ΔE_{AT} values in Table II. It is apparent that neither simple FMO theory nor the BEP principle are capable to pattern the data (compare, e.g., entries 2 vs. 3, 2 vs. 7, 7 vs. 8, 2 vs. 4, etc.).

The transition states for the attack phase appear in Table III and are all quite close to the average structure shown in **4**. In

4
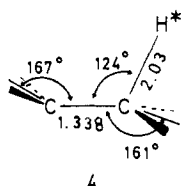
all these structures the leaving-group linkages (C–F, C–Cl) partake to only a small extent (ca. ~1–3%) in the activation. Note that this is true also for the single-step reaction 7.

The main features of the transition state (TS) in **4** are the trajectory by which the nucleophile (H*) approaches the olefin ($\angle H^*CC \geq 120°$) and the anti-type bending that the olefin undergoes about its two termini. These features have been observed in previous studies by Houk and co-workers[12] and by Bach and Wolber,[8a] as well as in studies of other nucleophilic addition reactions.[12,27] The results show that the olefin has to *invest a distortion effort of a particular kind* in order to reach the transition state. This distortion effort involves little or no internal rotation about the C–C axis (see θ values in Table III), even in the single-step reaction (7).

The computed TS geometries exhibit variations that do not seem to yield to any simplified argument of either the Hammond postulate[28] or the FMO theory (compare olefinic distortions and C–H* distances of reactions 4 vs. 6; compare C–H* distance of

reaction 7 to those of any other reaction; compare reactions 2 vs. 3, which possess the same π^* level and ΔE_{AT}, reactions 7 vs. 8, and 2 and 3 vs. 4). TS geometries and attack barriers seem thus to share common problems which require an explanation.

Conformational Phase (CP). The geometries of the A_1 and A_2 carbanions (see **3** above) are collected in the supplementary material. Reactions 1, 3–6, and 8 (Tables I and II) exhibit both A_1 and A_2 carbanions as real minima. On the other hand, $ClCH_2CH_2{}^-$ (reaction 7) does not possess any real minima, while $FCH_2CH_2{}^-$ (reaction 2) exhibits only an A_2 form, where the carbanionic electron pair occupies an antiperiplanar arrangement to the C–F bond ($FCH_2CH_2{}^-$ was located with the 3-21G and 6-31G* bases but not with 4-31G[8b,29]). These stability trends of the carbanions form the basis for the mechanistic spectrum, which is summarized above in Table I.

The $A_1 \rightarrow A_2$ transformation (CP in **3**) controls the stereochemical outcome of the substitution. The detailed process was studied for the substitution reaction of F^- from $H_2C{=}CHF$ (reaction 2, Table I) by following the minimum-energy pathway of the constrained A_1 carbanion ($60°$ in **5**) toward the second A_2

5
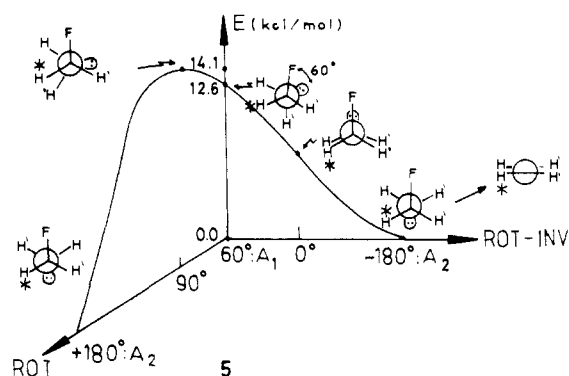
carbanion ($\pm180°$ in **5**). The results, which are plotted schematically in **5**, are in accord with previous studies[8] and follow the pathway that maximizes the hyperconjugative interactions as discussed in the literature.[11]

The A_1 carbanion (A_1, $60°$) is converted to the anti carbanion (A_2, $-180°$), following the downhill pathway through a syn carbanion ($0°$) which then undergoes a pyramidal inversion, about the $H_2C{:}^-$ center, to yield the anti carbanion (A_2, $-180°$). This barrierless rotation–inversion mechanism (ROT–INV) is preferred over the direct rotation mechanism (ROT), which must pass via the high energy $90°$ conformation. Note that the ROT–INV mechanism also preserves the isomeric identity of the olefin (see in **5**: primed H's remain cis in the final olefin on the right-hand side). The same mechanism operates for the single-step reaction (reaction 7)[8a] and seems to be in accord with the experimental data that show that unactivated olefins undergo substitution with retention of the olefin configuration.[1,30]

Expulsion Phase (El). The barriers for leaving-group expulsion ($E_{El}{}^*$) are collected in Table I. The TS geometries for F^- expulsion (reactions 2, 5 and 6) were difficult to locate. Only approximate structures were obtained, hence, for reactions 5 and 6 and are shown in **6a** and **6b** ($E_{El}{}^*$ values in parentheses). The negative

6A (0.8 kcal/mol)   **6B (0.3 kcal/mol)**
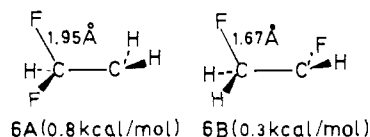
barrier for $ClCH_2CH_2{}^-$ in Table 1 means that the carbanion does

(25) (a) Koch, H. F.; Koch, J. G.; Koch, N. H.; Koch, A. S. *J. Am. Chem. Soc.* **1983**, *105*, 2388. (b) Koch, H. F.; Koch, J. G.; Donovan, D. D.; Toczko, A. G.; Kielbania, A. J., Jr. *J. Am. Chem. Soc.* **1981**, *103*, 5417.
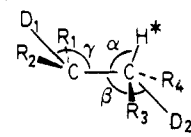
(26) Truce, W. E.; Boudakian, M. M. *J. Am. Chem. Soc.* **1956**, *78*, 2748. Truce, W. E.; Kassinger, R. *J. Am. Chem. Soc.* **1958**, *80*, 1916.

(27) (a) Eisenstein, O.; Hoffmann, R. *J. Am. Chem. Soc.* **1980**, *102*, 6148. (b) Nguyen, T. A.; Eisenstein, O. *Tetrahedron Lett.* **1976**, *88*, 146. (c) Bürgi, H.; Lehn, J. M.; Wipff, G. *J. Am. Chem. Soc.* **1974**, *96*, 1956.

(28) Hammond, G. S. *J. Am. Chem. Soc.* **1955**, *77*, 334.

(29) Schleyer, P. v. R.; Kos, A. J. *Tetrahedron* **1983**, *39*, 1141.

(30) (a) Aguiar, A. M.; Daigle, D. *J. Am. Chem. Soc.* **1964**, *86*, 2299. (b) Aguiar, A. M.; Daigle, D. *J. Org. Chem.* **1965**, *30*, 2826. *Ibid.* **1965**, *30*, 3527. Aguiar, A. M.; Archibald, T. G. *J. Org. Chem.* **1967**, *32*, 2627. (c) Park, D. J.; Cook, E. W. *Tetrahedron Lett.* **1965**, 4853. (d) Burton, D. J.; Krutzsch, H. C. *J. Org. Chem.* **1971**, *36*, 2351. (e) Normant, J.; Sauvetre, R.; Villieras, J. *Tetrahedron* **1975**, *31*, 891. (f) Sauvetre, R.; Normant, J.; Villieras, J. *Ibid.* **1975**, *31*, 897.

**Table III.** Transition State (TS) Geometries (4-31G) for the Attack Phase of Nucleophilic Substitution Reactions[a]

$\not\prec R_1 C R_2 = \delta$

$\not\prec R_3 C R_4 = \omega$

$\not\prec D_1 CCH^* = \theta$

	bond lengths, Å						angles, deg					
TS	CH*	CC	CR_1	CR_2	CR_3	CR_4	α	β	γ	δ	ω	θ
(1) $R_1 = R_2 = R_3 = R_4 = H$	1.896	1.367	1.078		1.070		124.0	156.0	165.2	115.3	113.7	0.0
(2) $R_1, R_2, R_3 = H$; $R_4 = F$	2.110	1.335	1.072	1.071	1.056	1.389	121.6	159.8	169.5	118.6	112.1	6.1
(3) $R_2, R_3, R_4 = H$; $R_1 = F$	1.969	1.345	1.432	1.062	1.065	1.065	124.6	158.2	162.6	110.0	116.3	3.8
(4) $R_1, R_2 = F$; $R_3, R_4 = H$	2.073	1.330	1.385		1.061		125.6	162.8	161.0	107.5	118.2	0.0
(5) $R_1, R_2 = H$; $R_3, R_4 = F$	b											
(6) $R_1, R_4 = F$; $R_2, R_3 = H$	2.160	1.325	1.403	1.064	1.054	1.370	122.4	162.1	168.6	112.5	114.7	10.3
(7) $R_1, R_2, R_3 = H$; $R_4 = Cl$	1.882	1.331	1.070	1.074	1.053	1.882	122.1	161.6	171.2	117.6	110.2	10.8
(8) $R_1, R_3, R_4 = H$; $R_2 = Cl$	2.117	1.331	1.063	1.890	1.063	1.065	126.4	168.7	169.6	108.9	116.3	5.6

[a] C–D lines are projections of C–C unto the corresponding RCR planes. [b] No TS found. Energy decreases monotonically toward $HF_2C-CH_2^-$.

not exist, and expulsion is a downhill energetic process.

According to Table I, the ease of expulsion follows the order shown in **7** below. Thus, the greater the hyperconjugative


7 (EASE OF EXPULSION)
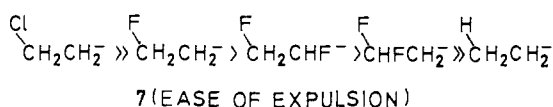
"stability" of the carbanion, the smaller its expulsion barrier. And this, as are the rest of the computational results, seems to be in accord with experimental data,[1b,10] and, hence, the computations may be considered reliable.

State Correlation Diagram Model

The key to unification of the above data is a methodology of constructing reaction profiles in a manner that reveals the origins of the various barriers.[13,14] We therefore begin with the construction of a profile for a stepwise reaction (see **3** above). With this as a basis, the requirements for the merging of all the phases into a *single step* will be derived and the various reaction barriers will be discussed. In what follows hereafter the various symbols used above in **3** will be utilized *throughout the discussion*, with one exception: the notation N:⁻ will replace H:⁻ to denote a general nucleophile.

Construction of Potential Energy Curves. Origins of Barriers. The potential energy profile for the attack (AT) phase has been discussed before[13] and is described in Figure 1. The reaction profile is generated by an avoided crossing of two curves that start out—from an encounter distance—as the ground and π-type *charge transfer* (π-CT) states of the reactants. The π-CT state contains the Heitler–London bonding scheme of the carbanion A_1. This is conveyed by either the MO or VB (valence bond) representations of π-CT in **8A** and **8B**. In both representation,

8A (N:̈:C bond pair)   8B (N:̈:C bond pair)

8C
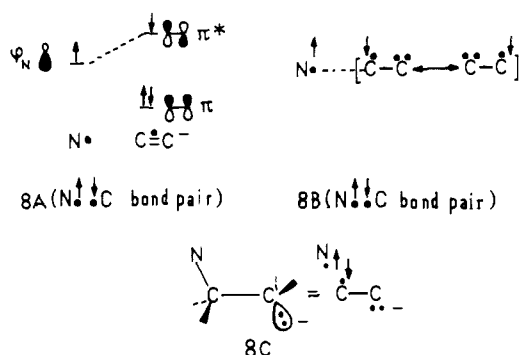
π-CT *contains* the electronic distribution of the carbanion A_1 in **8C**. Thus there exists, in either **8A** and **8B**, two spin-paired electrons (a *bond pair*) to match those in the N–C bond of A_1(**8C**), and an electron pair on the other carbon to match the carbanionic lone pair of A_1. The π-CT state is therefore the electronic template of the carbanion A_1 *but in the geometry of the reactants*. Hence,
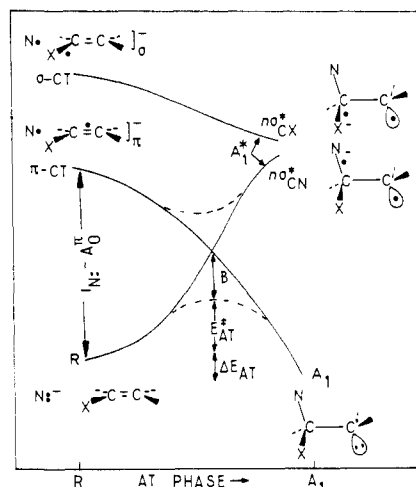

Figure 1. State correlation diagram for the attack (AT) phase (see **3**). Avoided crossing is shown by the dashed lines. *B* is the crossing avoidance interaction. Interaction of the $n\sigma^*$ configurations is deleted to preserve clarity.

as appropriate geometric reorganization takes place along the "reaction coordinate", a π-CT ⤳ A_1 correlation will be established as shown in Figure 1.[31a]

Along the same "reaction coordinate" the ground state of the reactants (R) will correlate with a specific excited configuration, A_1^*, of the A_1 carbanion. This excited configuration is qualified in Figure 1 as A_1^* ($n\sigma^*_{CN}$) to convey the specific electronic promotion that relates A_1^* to A_1. The rationale for the R ⤳ A_1^* ($n\sigma^*_{CN}$) correlation is exactly equivalent to that presented above for the π-CT ⤳ A_1 correlation.

The so obtained state correlations lead to two intersecting curves whose avoided crossing generates the transition state and the barrier ($E_{AT}^{\ddagger}$) for the attack phase. The origin of the barrier is thus clear: the N:⁻/RR′C=CR″X → NRR′C–ĊR″X⁻ transformation involves an interchange of *two distinct bonding schemes*. This interchange can be established *only by crossing* whose avoidance (in Figure 1) generates a barrier.

The similarity of the attack phase to the S_N2 reaction[13,14] becomes obvious once a comparison is made between the corresponding correlation diagrams. In accord with this analogy, the attack phase can be defined as a transformation that involves *a single electron shift* ($N:⁻ →$ olefin) *that is synchronized with rehybridization and bond interchange*.

Figure 1 contains a third curve that begins as the σ-CT state, at the reactant (R) side, and correlates with the A_1^* ($n\sigma^*_{CX}$)

(31) (a) The π-CT → A_1 correlation is completed by the mixing in of additional configurations into π-CT. See details in ref 13. (b) At each geometry the two $n\sigma^*$ type forms mutualy mix. However, $A_1^*(n\sigma_{CN}^*)$ will involve a major $n\sigma_{CN}^*$ character while $A_2^*(n\sigma_{CX}^*)$ a major $n\sigma_{CX}^*$ character.
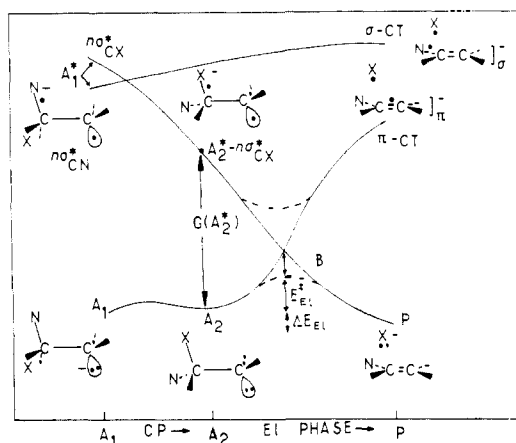
Figure 2. State correlation diagram for CP and El phases (see 3). Avoided crossing is shown by the dashed lines. Interactions of A_1 and A_2 with A_1^* and A_2^* are deleted to preserve clarity.
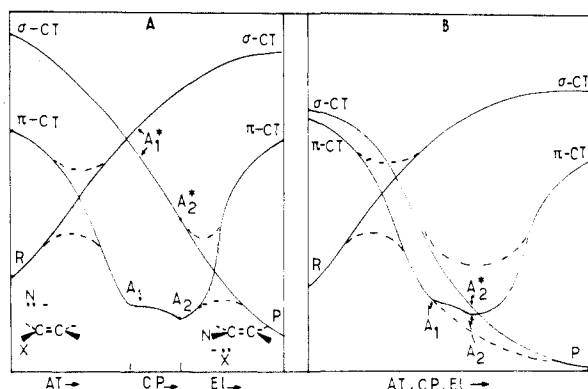

Figure 3. State correlations diagrams including all reaction phases. (a) A situation that leads to a stepwise mechanism. (b) A situation that leads to a single-step reaction. Avoided crossings in (a) and (b) are shown by dashed lines.

configuration of the A_1 carbanion. This curve becomes all important, past the attack phase, as shown in Figure 2, which describes the conformational (CP) and expulsion (El) phases.

The conformational phase $A_1 \rightarrow A_2$ involves no avoided crossings since all bonds and electron pairs remain intact. The relative energies of A_1 and A_2 depend on the strengths of the $A_1-A_1^*$ and $A_2-A_2^*$ stabilizing interactions. Thus the carbanion A_1 is stabilized by mixing mainly some (λ) of the A_1^* ($n\sigma^*_{CN}$) configuration as shown in **9A**, while A_2 is stabilized by the cor-

9
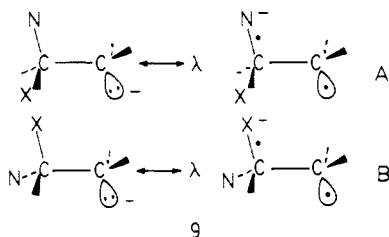
responding mixing[31b] of A_2^* ($n\sigma^*_{CX}$) as shown in **9B** (see e.g., the relative stabilities of A_1 and A_2 for $FCH_2CH_2^-$ in **5** above). These interaction types are well-known in their MO versions as hyperconjugative interactions.

The expulsion phase (El) in Figure 2 begins with the carbanion A_2. This phase is really a reverse-type process of the attack phase (Figure 1), and therefore, the expulsion profile is generated by the same type of state correlations as is the attack phase. The excited configuration A_2^* ($n\sigma^*_{CX}$) is the electronic template of the product (P in Figure 2) because both contain equivalent electronic distributions, though in different geometries as shown in **10**. Thus, A_2^* ($n\sigma^*_{CX}$) will correlate with the ground state of the substitution product as changes in geometry occur along the expulsion "reaction coordinate". At the same time, the ground

10 $(A_2^* - n\sigma^*)$
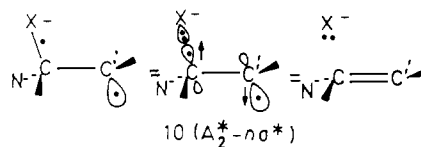
state of the carbanion, A_2, will correlate with the π-CT state of the product.

The avoided crossing of the two curves generates the transition state and the barrier for leaving-group expulsion (E_{El}^*) as shown in Figure 2. Thus the expulsion process can be described as *a transformation that involves a single electron shift—from the carbanionic center to the C–X bond—synchronized with rehybridization and bond interchange.* Again the similarity to S_N2 is obvious.[13,14]

Stepwise vs. Single-Step Substitution. As we have seen in Table I, the π-oriented attack shown in **11** leads to both stepwise and

11
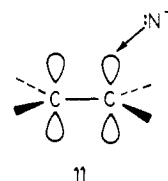
single-step reactions. To derive the conditions for the two mechanisms, the various reaction phases of Figures 1 and 2 are integrated into single diagrams in Figure 3 parts A and B.

The mechanistic identity of a given reaction will be determined by the proximity of the two energy curves that begin as σ-CT and π-CT in Figure 3. Thus, a large separation of σ-CT and π-CT, as in Figure 3A, leads to a stepwise mechanism with discrete attack and expulsion phases (AT, El). Such a case arises whenever the acceptor ability of the C–X bond is much weaker than that of the π-bond (consult the corresponding structures in Figure 1). On the other hand, whenever the C–X acceptor ability is close to that of the π-bond, a single-step mechanism will take place, as shown in Figure 3B. Note that the reverse reaction of such a case involves also a single-step mechanism. Thus, in general, the mechanistic identity of the reaction will be determined also by the nucleophile. It follows then, that small gaps between the σ-CT and π-CT curves at either the reactant or the product ends (R and P) will cause single-step substitutions.

To utilize Figure 3 for rationalizing the nature of reactions 1–8 (Table I) it is sufficient to calibrate the energy gaps at the reactant side (R) and at the geometry that is specified by A_2. At the reactant side, the π-CT/σ-CT gap is given by the electron affinity difference ($A_0^\pi - A_{CX}$) of the π(C≡C) and σ(C–X) bonds, where X is the leaving group. These energy gap values are collected in Table IV. As can be seen from entries 1–5, the π-CT and σ-CT states of the reactants will be fairly well separated, as in Figure 3A, when the leaving group X is either H or F. However, when X = Cl the two states are almost degenerate, as in Figure 3B.

The second point that must be examined is the starting point of the expulsion phase, at the geometry represented by A_2 (Figures 2 and 3). The requisite energy gap is $G(A_2^*)$, which can be expressed as follows:

$$G(A_2^*) \approx I_{C:} - A_{CX} - fD^\pi_{C=C} \qquad (f \sim 0.5) \qquad (2)$$

Here $I_{C:}$ is the ionization potential of the carbanionic center of A_2 and A_{CX} is the electron affinity of the C–X bond of the carbanion. The last term in eq 2 is a fraction (f) of the π-bond energy ($D^\pi_{C=C}$). This term takes into account the fact that in the A_2 geometry the two odd electrons of A_2^* are coupled (see **10**) to generate a π-bond whose strength is fractional (f) relative to π-bond in a relaxed olefin. If we make the simplifying and safe[32]

(32) From overlap considerations, A_2^* has $\sim 50\%$ π-bond. Also, the assumption ($f = 0.5$) reproduces the trends and the approximate numerical values of the rotation barriers in the constrained $FCH_2CH_2^-$ and $ClCH_2CH_2^-$. Using $f = 0.5$, we calculate barriers of 8.5 and 15 kcal/mol, respectively (while STO-3G computes barriers of 10 and 16.7 kcal/mol in ref 11a and 3-21+G yields 10.2 kcal/mol for $FCH_2CH_2^-$ in ref 29).

Table IV. $(A_0^\pi - A_{CX})$ Energy Gaps for Olefins and $G(A_2^*)$ Energy Gaps for Carbanions

N⁻/olefin	$(A_0^\pi - A_{CX})^{a,b}$	carbanion	$G(A_2^*)^{a,c,d}$
(1) H⁻/H₂C=CH₂	49 (X = H)	HCH₂CH₂⁻	63
(2) H⁻/H₂C=CHF	20 (X = F)	FCH₂CH₂⁻	29
(3) H⁻/H₂C=CHCl	2 (X = Cl)	ClCH₂CH₂⁻	0
(4) H⁻/HFC=CFH	14 (X = F)	FCH₂CHF⁻	36
(5) H⁻/H₂C=CF₂	19 (X = F)	FCHFCH₂⁻	29
(6) H⁻/PhCH=CHF	58 (X = F)	FCH₂CHPh⁻	49–59
(7) H⁻/PhCH=CHCl	25 (X = Cl)	ClCH₂CHPh⁻	20–30
(8) H⁻/PhCH=CHBr	15 (X = Br)	BrCH₂CHPh⁻	10–20
(9) H⁻/PhCH=CHI	5 (X = I)	ICH₂CHPh⁻	0–10
(10) H⁻/NCCH=CHF	60 (X = F)	FCH₂CHCN⁻	64–74
(11) H⁻/(NC)₂C=CHF	89 (X = F)	FCH₂C(CN)₂⁻	84–94
(12) F⁻/PhCH=CHCl	25 (X = Cl)	Cl₂CHCHPh⁻	20–30
(13) I⁻/PhCH=CHCl	25 (X = Cl)	IClCHCHPh⁻	0–10
(14) R₂P⁻/ClCH=CHCl	6 (X = Cl)	Cl(PR₂)CHCHCl⁻	13
(15) RO⁻/ClCF₃C=CCF₃Cl	>10 (X = Cl)	Cl(OR)CF₃CCCF₃Cl⁻	>40

a In kcal/mol. *b* A_{CX} values are estimated as in ref 14d,g (see supplementary material). A_0^π values are from ref 3 (entries 1–5; 14) and 33a (entries 6–13; 15). *c* Obtained from eq 2 ($D_{C=C}^\pi$ = 60 kcal/mol for all the olefins, except for PhCH=CHX, NCCH=CHX, and (NC)₂C=CHX, for which this value is 50–60 kcal/mol). *d* I_{C} values are from ref 33b (see supplementary material).

assumption that $f = 0.5$ in eq 2, we can then estimate trends in $G(A_2^*)$. These values are collected in the last column of Table IV and show that the two curves are well separated ($G(A_2^*) > 0$) in all the cases for which X = H or F. Hence, the expulsion phase for these cases fits the description given in Figure 3A. On the other hand, when X = Cl, the two curves are touching ($G(A_2^*) \sim 0$) and thereby they fit the description in Figure 3B.

These trends rationalize the mechanistic qualifications given before in Table I for reactions 1–8. Thus all the reactions whose leaving groups X are either H or F resemble Figure 3A, and, hence, they exhibit a stepwise mechanism (reactions 1–6 and 8, Table I). On the other hand, when the leaving group X is Cl there results a single-step mechanism (reaction 7, Table I) in accord with the characteristics of Figure 3B.

The energy curves could be similarly calibrated for other system by using known electron-affinity data.[33] Some representative cases are shown, alongside their corresponding energy gaps, in entries 6–15 of Table IV. As can be seen from entries 6–9, for a given olefin the energy gaps decrease as the leaving group changes from X = F to X = I. For a given leaving group, the gap decreases as the β-substituent becomes an inferior π-acceptor (less activating), i.e., (NC)₂ > NC > Ph (entries 11, 10, and 6). Finally, for a given olefin the $G(A_2^*)$ gap decreases as the nucleophile is changed to one that forms low σ-CT states in the substituted products (entry 12 vs. 13).

The likelihood of a single-step mechanism increases as the above gaps decrease in magnitude. Therefore, likely candidates to undergo single-step substitution are β-iodo- and β-bromostyrenes (entries 8 and 9) and the ClCH=CHCl olefins (entry 14). On the other hand, the activated systems (entries 10 and 11), β-fluorostyrene (entry 6) and the ClF₃CC=CCF₃Cl olefins (entry 15) are likely to exhibit a stepwise mechanism. These conclusions are in accord with the corresponding experimental data.[1a,b,30] Yet these data must be interpreted with care, since partial stereoconvergence is a positive evidence, while stereospecificity (retention) may well be common to single step as well as to stepwise mechanisms (see 5 above).[8a,11]

In general, the present conclusions match the guidelines that have been recently summarized by Rappoport.[1b] Still an interesting possibility arises to investigate the mechanistic choice of weakly activated systems as a function of the nucleophile (e.g., entry 12 vs. 13).

(33) (a) A_0^π values for olefins are taken from: Jordan, K. D.; Burrow, P. D. *Acc. Chem. Res.* **1978**, *11*, 341. (b) I_{C} values are the electron affinities of the corresponding radicals and are tabulated in: Janousek, B. K.; Brauman, J. I. In "Gas Phase Ion Chemistry"; Bowers, M. T., Ed.; Academic Press: New York, 1979; Chapter 10 (for CH₃, CH₂CN, CH₂Ph). McMahon, T. B.; Kebarle, P. *J. Am. Chem. Soc.* **1976**, *98*, 3399 (for C(CN)₂H). Sullivan, S. A.; Beauchamps, J. L. *J. Am. Chem. Soc.* **1976**, *98*, 1160 (CHFCF₃ and related radicals). Bartmess, J. E.; McIver, R. T., Jr. In "Gas Phase Ion Chemistry"; Bowers, M. T., Ed.; Academic Press: New York, 1979; Vol. 2, Chapter 11 (CF₃, CCl₃).

Energy Barriers. *Attack Phase.* The barrier for attack $(E_{AT}^\ddagger)$ is seen from Figure 1 to be a fraction—f—of the electron-transfer gap $(I_{N:} - A_0^\pi)$ less the crossing avoidance interaction, B

$$E_{AT}^\ddagger = f(I_{N:} - A_0^\pi) - B \qquad (3)$$

The fraction—f—reflects the curvature of the two intersecting curves and is domianted by the reaction energy, ΔE_{AT}, as well as by the *steepness of descent* of π-CT and A_1^* ($n\sigma^*_{CN}$) toward the crossing point of Figure 1. Such factors have been extensively discussed in our S_N2 studies,[14] and as has been shown there the resulting form of the barrier becomes approximately the following:

$$E_{AT}^\ddagger \simeq f'(I_{N:} - A_0^\pi)^2/[(I_{N:} - A_0^\pi) - \Delta E_{AT}] - B \qquad (4)$$

where f' is the fraction f at $\Delta E_{AT} = 0$. And therefore f' accounts only for the effect of *steepness of descent* mentioned above.

The two upper states π-CT and A_1^* ($n\sigma^*_{CN}$) in Figure 1 descend toward the crossing point owing to the bond coupling interaction between the two odd and spin-paired electrons that are possessed by these states. For example, as shown above in **8A**, π-CT possesses a bond pair. As the nucleophile (N) approaches the olefin, the bond-pair electrons will be gradually coupled to an N–C bond and thereby π-CT descends toward the crossing point of Figure 1. The strength of the bond-coupling interaction in π-CT depends on the π-odd electron density at the sites of attack of N· and $(C_1\dot{=}C_2)^-$. And hence, the delocalization properties of π-CT will determine its steepness of descent toward the crossing point of Figure 1. The same argument applies to the A_1^* state.[34]

To exemplify, let us focus on the radial anion $(C_1\dot{=}C_2)^-$ where the odd electron is delocalized over the two centers C_1 and C_2. The bond-coupling interaction of any one of the centers with N· will then be weak, in comparison with an interaction of N· with a localized Ċ-Ċ. Such a weakening will exert a drastic effect on the descent of π-CT as shown in **12A** and **12B**. The delocalization

12A (small f⁻)   12B (large f⁻)
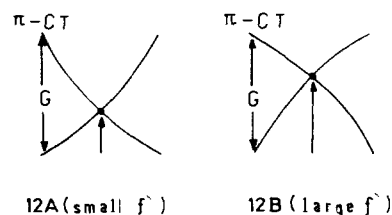
of $(C_1\dot{=}C_2)^-$ thus shifts the crossing point to a higher energy (**12B** vs. **12A**) and thereby leads to a higher f' factor in eq 4 for a given gap G).

Consider now a radical anion that possesses the VB makeup shown in eq 5, where W_1 and W_2 are weights of the corresponding

$$(C_1\dot{=}C_2)^- = W_1(\dot{C}_1—\ddot{C}_2) + W_2(\ddot{C}_1—\dot{C}_2) \qquad W_1 + W_2 = 1 \qquad (5)$$

(34) Other factor such as overlap repulsion (steric), electrostatic, etc., also contribute to f but are not discussed here explicitly. See details in ref 14g.

Table V. Reactivity Factors and Barriers (kcal/mol) for Reactions 1–8

reacn	reactivity factors[a]		DZ//4-31G results		calcd barriers	
	$I_{H:} - A_0^\pi$	$(f' = 1 - W_1)^b$	ΔE_{AT}	$E_{AT}^\ddagger$	$E_0^\ddagger$ (eq 10)	$E_{AT}^\ddagger$ (eq 9)
(1) $H^- + H_2C=CH_2 \rightarrow CH_3CH_2^-$	58.91	0.500	−16.03	12.65	15.45	9.15
(2) $H^- + H_2C=CHF \rightarrow FCH_2CH_2^-$	61.44	0.481	−29.55	6.93	15.55	5.96
(3) $H^- + H_2C=CHF \rightarrow CH_3CHF^-$	61.44	0.519	−27.33	9.90	17.89	8.07
(4) $H^- + H_2C=CF_2 \rightarrow CH_3CF_2^-$	72.51	0.578	−47.31	6.76	27.91	11.36
(5) $H^- + H_2C=CF_2 \rightarrow F_2CHCH_2^-$	72.51	0.422	−46.77	<0[d]	16.60	4.60
(6) $H^- + HFC=CHF \rightarrow FCH_2CHF^-$	67.67	0.500	−46.13	2.69	19.83	6.11
(7) $H^- + H_2C=CHCl \rightarrow H_2C=CH_2 + Cl^-$	46.92	0.762[c]	e	7.91	21.75	e
(8) $H^- + H_2C=CHCl \rightarrow CH_3CHCl^-$	46.92	0.738[c]	−47.60	0.52	20.61	3.19

[a] $I_{H:} = 17.4$ kcal/mol. A_0^π are from ref 3. [b] From eq 6 with $k = 1$. The index 1 signifies the site of attack. [c] For the π component see eq 12. The present values derive from eq 12 and 13. [d] Energy decreases monotonically. [e] ΔE_{AT} is not available. The use of $\Delta E_{AT} = -29.55$ kcal/mol leads to $E_{AT}^\ddagger = 7.94$ kcal/mol.

VB structures. For an attack on C_1, the N–C bond-coupling interaction will be weakened in proportion to the value of W_2 because $\ddot{C}_1$-$\ddot{C}_2$ does not contribute to N–C_1 bonding but rather to repulsion owing to the 3-electron interaction (N· with $\ddot{C}_1$).[14] Therefore, for an attack on C_1, the f' factor is proportional to W_2

$$f'(C_1) = kW_2 = k(1 - W_1) \qquad k = \text{proportionality constant} \tag{6}$$

In fact, any substituent that further delocalizes the odd π-electron away from the site of attack C_1 will further weaken the N–C_1 bond-coupling interaction with a consequential increase of f' (see **12B** vs. **12A**). Thus, in general f' will be proportional to the *sum of the weights* of all the VB configurations that describe the radical anion *but that do not place the odd electron on the site of attack*, C_1. Substituting the expression of f' into eq 4 one obtains eq 7 for the attack barrier on a specified olefinic site C_1.

$$E_{AT}^\ddagger(C_1) \simeq k(1 - W_1)[(I_{N:} - A_0^\pi)^2/\{(I_{N:} - A_0^\pi) - \Delta E_{AT}\}] - B \tag{7}$$

An "intrinsic barrier" can be defined by setting ΔE_{AT} to zero in eq 7 to obtain[35]

$$E_0^\ddagger \simeq k(1 - W_1)(I_{N:} - A_0^\pi) - B \tag{8}$$

One can then utilize eq 7 and 8 to treat separately the effects of the so-called "kinetic" barrier $(E_0^\ddagger)$ and the thermodynamic "driving force". To apply the model to the computational results a simplifying assumption is made that the crossing avoidance, B, is a constant, 14 kcal/mol, and $k = 1$, exactly as was assumed in the S_N2 studies.[14e,g] The "quantitative" equation then reads

$$E_{AT}^\ddagger(C_1) \simeq (1 - W_1)(I_{N:} - A_0^\pi)^2/[(I_{N:} - A_0^\pi) - \Delta E_{AT}] - 14 \tag{9}$$

$$E_0^\ddagger(C_1) \simeq (1 - W_1)(I_{N:} - A_0^\pi) - 14 \tag{10}$$

Reactivity factors and barriers for the eight computed reactions are collected in Table V. The delocalization indices $(1 - W_1)$ have been obtained with a simple VB scheme such as the one utilized in the S_N2 studies.[14] For example, $(H_2C=CHF)^-$ is described by (see supplementary material)

$$(H_2C=CHF)^- = 0.519(H_2\ddot{C}-\dot{C}HF) + 0.481(H_2\dot{C}-\ddot{C}HF) \tag{11}$$
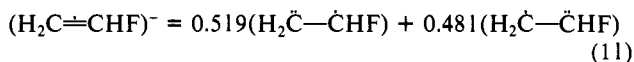
A similar trend is obtained for $(H_2C=CF_2)^-$, for which the weights W_1 and W_2 are 0.578 and 0.422, correspondingly. Within our VB scheme the electronic distributions of $(H_2C=CHF)^-$ and $(H_2C=CF_2)^-$ derive from the fact that in a planar geometry, fluorine tends to slightly destabilize an adjacent electron pair.[1f] As a result, the $H_2\ddot{C}-\dot{C}HF$ and $H_2\dot{C}-\ddot{C}F_2$ configurations become less stable than the corresponding ones which have the odd electron localized on the substituted carbon. This electronic distribution

is in accord with the computed (UHF/4-31G) spin densities of these radical anions.

Chlorine exerts exactly an opposite effect than that of fluorine. Since Cl stabilizes adjacent carbanions even in a planar geometry,[1f] the $H_2\ddot{C}-\dot{C}HCl$ configuration is slightly more stable relative to $H_2\dot{C}-\ddot{C}HCl$. Thus the odd electron in $(H_2C=CHCl)^-$ tends to be localized more on the CH_2 terminus, and this is the reason why the $1 - W_1$ index for attack at the CH_2 terminus is smaller than for attack on the CHCl teminus (entries 7 vs. 8, Table V), as shown in eq 12

$$(H_2C=CHCl)^- = 0.476(H_2\ddot{C}-\dot{C}HCl) + 0.524(H_2\dot{C}-\ddot{C}HCl) \tag{12}$$
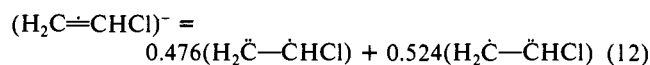
The radical anion of $H_2C=CHCl$ undergoes however an additional mode of delocalization that is absent in fluoro olefins. As we have seen above in Table IV, the π and σ(C–Cl) radical anions are almost degenerate $(A_0^\pi - A_{CCl} = 2$ kcal/mol). Therefore a slight deviation from planarity would mix the two anionic states, so that a more reliable description of $(H_2C=CHCl)^-$ for our purposes is (0.5 is the square of the coefficient)

$$(H_2C=CHCl)^-\!\cdot \simeq 0.5[(H_2C=CHCl)^-] + 0.5[(H_2C=CH-Cl)^-] \tag{13}$$
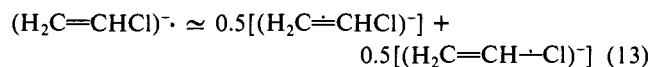
Thus, Cl causes delocalization of the odd electron into the C–Cl linkage, and therefore the π-oriented attacks on $H_2C=CHCl$ will have larger $1 - W_1$ indices than do fluoro olefins, as can be wittnessed from Table V (entries 7 and 8 vs. 1–6).

The calculated "intrinsic barriers" $(E_0^\ddagger)$ for reactions 1–8 of the present study are collected in Table V. Large gaps $(I_{H:} - A_0^\pi)$ and delocalization indices (f') are seen to generate high "intrinsic barriers" (see, e.g., entries 5 vs. 1 and 7 and 8 vs. 2 and 3).

The attack barriers $E_{AT}^\ddagger$ are calculated in the last column of Table V according to eq 9. The correspondence to the computed values (DZ//4-31G) is fair, but the trends are instructive. Thus, the enhanced reacttivity of $H_2C=CF_2$ (entry 5) is conspired by a low $E_0^\ddagger$ owing to favorable localization of the odd electron on the CF_2 teminus of $(H_2C=CF_2)^-$ and by a favorable thermodynamic driving force (ΔE_{AT}) relative to the other fluoroethylenes. The barrier for $H^-/H_2C=CH_2$ is larger than that for $H^-/FHC=CFH$(entries 1 vs. 6) despite the reverse order of their $E_0^\ddagger$'s. The root cause of this inversion is seen to be the thermodynamic "driving force", ΔE_{AT}, which favors $H^-/FHC=CHF$. A similar rationale accounts for the inferior reactivity of $H_2C=CH_2$ relative to all the fluoroolefins (entry 1 vs. 2,3,5 and 6). Similarly, reaction 8 ($H^-/H_2C=CHCl$) has a low barrier despite the large $E_0^\ddagger$, precisely because the thermodynamic "driving force" is so great $(\Delta E_{AT} = -47.6$ kcal/mol).

The regiochemical preferences of attack on $H_2C=CHF$ and $H_2C=CF_2$ (entries 2 vs. 3 and 4 vs. 5) result primarily from the trends in the corresponding "intrinsic barriers". These trends originate in the tendency of fluorine to localize the odd electron on the F-substituted center. In contrast, the "intrinsic barriers" of reactions 7 and 8 suggest that part of the regiochemical preference of attack on $H_2C=CHCl$ is contributed by the tendency of chlorine to localize the odd electron away from the Cl-

(35) Marcus, R. A. *J. Chem. Phys.* **1968**, *72*, 891.

Table VI. Stabilization Energy (kcal/mol) of Radical Anions upon Anti Type Bending and Other Distortions

radical anion	ΔE(planar → bent)[a]	ΔE(planar → planar optimized)[a,c]	ΔE(planar → perpendicular)[b]
(1) $H_2C=CH_2^-$	-11.96 (-13.0^b)	-9.3^b	$+13.5^b$
(2) $H_2C=CHF^-$	-15.92 (-22.9^b)	-12.5^b	
(3) $H_2C=CF_2^-$	-40.46	-14.91	
(4) $HFC=CFH^-$	-38.03		
(5) $H_2C=CHCl^-$	decomposes		

[a] UHF/4-31G computations with spin annihilation of quartet components. The anti type distortion is shown in **14** in the text. [b] UHF/3-21G result from: Paddon-Row, M. N.; Rondan, N. G.; Houk, K. N.; Jordan, K. D. *J. Am. Chem. Soc.* **1982**, *104*, 1143. [c] The planar optimized structures involve mainly CC elongation.

substituted center (eq 12). The ΔE_{AT} value certainly contributes[8a] to the overall regiochemical effect, but ΔE_{AT} is unavailable for reaction 7 (see footnote *e* in the table).

Similarly, comparing the "intrinsic barriers" of reactions 2 vs. 7 reveals that a possible origin of the DZ//4-31G computed "element effect" ($E_{AT}^{\ddagger}$(Cl) > $E_{AT}^{\ddagger}$(F)) is the excessive delocalization effect exerted by the chlorine substituent (eq 13). The same effect may contribute also to the generally observed lower reactivity of chloro olefins relative to fluoro olefins (e.g., Cl_2-C=CCl_2$ vs. $F_2C=CF_2$),[1f,g] though other effects (e.g., "steric")[1a,f,34] are certainly involved too.

The effect of delocalization vs. localization (f' in eq 4) has been recognized before by Bernasconi[5d] in his experimental studies of delocalized olefins and nucleophiles. Bernasconi and co-workers[5b,e] have shown for example that nitro-substituted olefins have higher "intrinsic barriers" than do cyano olefins (NO_2 will delocalize the odd electron away from the C=C moiety in the radical anion). Likewise, delocalized nucleophiles such as $(NC)_2CH^-$ are found[5a] to have higher "intrinsic barriers" than do localized nucleophiles like amines. The conclusion of Bernasconi that these high "intrinsic barriers" occur owing to a high degree of structural and solvational reorganization is supported by our model (computational evidence will be discussed in the section on TS geometry).

In summation, according to eq 4, trends in $E_{AT}^{\ddagger}$ will arise from an interplay of three main factors: (a) the delocalization properties, e.g., of $N\cdot/(RR'C=CR''X)^-$; (b) the electron-transfer energy gap ($I_{N:} - A_0^{\bullet}$) that in solution will involve also solvation and solvent reorganization terms;[14e] and (c) the reaction energy, ΔE_{AT}. Reaction series ($N:^-/RR'C=CR''X$) that are typified by a large delocalization index (f') will possess, in general, high "intrinsic barriers" and high selectivity. These trends are in complete analogy with S_N2 reactivity patterns.[14b,d,g]

Expulsion Phase. The barrier to leaving-group expulsion is seen from Figure 2 to be a fraction f of the energy gap $G(A_2^*)$ less the crossing avoidance B. Applying analogous arguments to those that were applied to the attack phase, the expression for the expulsion barrier, $E_{El}^{\ddagger}$, becomes

$$E_{El}^{\ddagger} \simeq f'[G(A_2^*)]^2/[G(A_2^*) - \Delta E_{El}] - B \qquad (14)$$

As above (**12A** vs. **12B**) f' takes into account the effect of odd electron delocalization in A_2^* as well as in π-CT of the product olefin. One type of such delocalization effect in A_2^* is shown in **13** in which one of the odd electrons is seen to be delocalized over
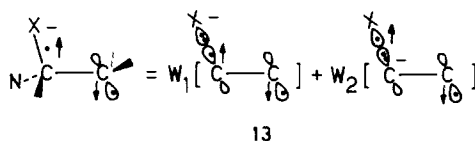
13

the two atomic centers of the C–X linkage. Increase of W_2 in **13** decreases the bond-coupling interaction across the C–C linkage and will thereby lead to an increase of f' in eq 14. In complete equivalence to the attack phase, this delocalization factor will set the size of the "intrinsic barrier", which reads

$$E_0^{\ddagger}(El) \simeq f'G(A_2^*) - B \qquad (15)$$

The rest of the barrier factors in eq 14 are $G(A_2^*)$, which reflects the electron-transfer gap ($A_2 \rightarrow A_2^*$ in Figure 2 and eq 2), and ΔE_{El}, which is the expulsion reaction energy.

The trends in the computed barriers, $E_{El}^{\ddagger}$, in Table I derive mainly from the $G(A_2^*)$ gaps that appear in entries 1–5 of Table IV. Thus, whenever the leaving group is H the $G(A_2^*)$ gaps are large with correspondingly large expulsion barriers. Fluorine and chlorine leaving groups have small to zero $G(A_2^*)$ gaps and, in accord, small or negative barriers (reactions 2,5,6, and 7 in Table I). The negative $E_{El}^{\ddagger}$ value corresponds to Cl^- expulsion, for which $G(A_2^*) \sim 0$. Such a "negative barrier" means that the avoided crossing results in a barrierless and downhill expulsion process, as described for single-step reactions in Figure 3B.

Other $E_{El}^{\ddagger}$ trends in Table I can be similarly understood by considering substituent effect on $G(A_2^*)$ in eq 2. Note that $G(A_2^*)$ determines also the hyperconjugative "stability" of the carbanion (see **9B**) and its rotational barrier. Thus, small $G(A_2^*)$ will lead to both small $E_{El}^{\ddagger}$ and large rotational barriers for the A_2 carbanion.

The above trends in the computed data have experimental parallels,[1b,10] many of which find a straightforward rationale by simply considering the $G(A_2^*)$ gap which resembles the corresponding HOMO–LUMO gap. These trends are well recognized and have been anticipated by Stirling.[10]

The interesting trends arise from variations in the delocalization index (f' in eq 14 and 15). The larger the f' index the greater usually the "intrinsic barrier". Modulation of f' can be achieved, for example, by substituents on the carbon bearing the leaving group. Substituents such as $Y = SR$, SO_2R, NR_3^+, Cl etc., in $X(Y)C(R)—CR'R''^-$ will increase f' through the enhancement of the W_2 weight in **13**. Substituents like $Y = OR$ and NR_2 will, on the other hand, decrease f' by diminishing this W_2 weight. Related examples could be the amine-catalyzed leaving group expulsions and the effect of $Y = SAr$ vs. $Y = OAr$ substituents, which have been discussed by Rappoport and co-workers.[1b,36]
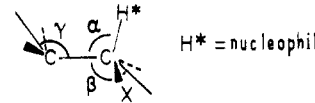
Variation of the leaving group X will also affect f', either through the increase of W_2 in **13** or through the delocalization properties of the π-CT state of the expulsion product (i.e., (C=C)/$\cdot$X in Figure 2). Cognizance of this latter delocalization effect has been taken before by Bernasconi and co-workers,[5c,e] who concluded that delocalized X^- leaving groups possess high "intrinsic barriers".

In summation, the trends in the barriers $E_{AT}^{\ddagger}$ and $E_{El}^{\ddagger}$ follow directly from the crossing requirements of Figures 1 and 2. As shown below the same requirements generate also the trends in TS geometries.

Transition-State Structure. Role of Distortions. As shown in Figure 1 the TS for attack is obtained from an avoided crossing of the ground ($N:^-/C=C$) and the π-CT ($N\cdot/(C=C^-)$ states. Since the two states are initially separated by an energy gap ($I_{N:} - A_0^{\bullet}$), *molecular distortions* will be required to lead to stabilization of the π-CT state and simultaneously to destabilization of the ground state, so that the two states wil achieve energy equality at the crossing point. The "reactive distortions" will be those that lead to the steepest descent of π-CT and simultaneously to the shallowest ascent of the ground state. In this manner there will result the *lowest possible* crossing point that defines the locus of the TS for the attack phase.

The requisite olefinic distortions can be predicted by considering all the possible modes that can stabilize the radical anion ($C=C)^-$ in π-CT (Figure 1). The energetics of radical anion distortions

(36) Rappoport, Z.; Avramovitch, B. *J. Org. Chem.* **1982**, *47*, 1397.

Table VII. Distortion Efforts in the Transition States, Barriers, and Reactivity Factors (kcal/mol) for Reactions 1-8

$H^* =$ nucleophile

	distortion efforts					barriers and reactivity factors			
reacn	% CH*[a]	% CC[b,c]	% β	% γ	% (β + γ)	$E_{AT}^{\ddagger}$	$I_{N:} - A_0^{\pi}$	f'	ΔE_{AT}
(1) H⁻/H₂C=CH₂	49.8 (30.3)	18.3 (3.9)	44.4	24.8	69.2	12.65	58.91	0.500	-16.03
(3) H⁻/H₂C=CHF	45.3 (20.8)	17.3 (3.1)	39.4	25.4	64.9	9.90	61.44	0.519	-27.33
(7) H⁻/ClHC=CH₂	51.1 (32.8)[d]	(1.9)				7.91	46.92	0.762	
(2) H⁻/FHC=CH₂	40.5 (9.6)[e]	14.7 (2.3)				6.93	61.44	0.481	-29.31
(4) H⁻/H₂C=CF₂	40.5 (9.6)	13.7 (2.4)	30.9	25.8	56.7	6.76	72.51	0.578	-47.31
(6) H⁻/FHC=CFH	37.2 (1.1)	13.8 (1.8)	34.2	17.9	52.1	2.69	67.67	0.500	-46.13
(8) H⁻/H₂C=CHCl	38.9 (5.6)	11.2 (1.9)	19.5	14.8	34.3	0.52	46.92	0.738	-47.60
(5) H⁻/F₂C=CH₂	~0[f]					<0	72.51	0.422	-46.77

[a] Bond order type index, % $n_{CH\cdot}$ = 100 exp[$(r_{A_1} - r^*)/r_{A_1}$], A_1 = carbanion. In parentheses % of CH* bond making where 100% CH* stretch relative to the carbanion is defined as 0% bond making. [b] 100[$r^*_{CC} - r_{CC}(R)$]/[$r_{CC}(A_1) - r_{CC}(R)$], R = reactant olefin. [c] In parentheses, percentages of CC bond lengthening relative to the olefin. [d] Assuming $r_{CH\cdot}$ = 1.09 Å in the nonexistent carbanion. [e] A_1 is optimized with constraint. [f] Very early crossing point, small distortion effort, and a "negative barrier".

are collected in Table VI for the five olefins of the study. As can be seen, the anti type bending mode shown in **14** leads to the

$$[\; {}^{-}\!C \!=\!\! C \ ]^{-} \; \longrightarrow \; [\; {}^{.}\!C \!=\!\! C^{.} \;]^{-}$$

14
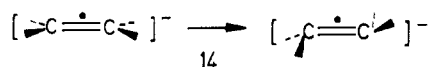
greatest stabilization. And in fact energy optimization of all the radical anions leads to anti type bent structures, in accord with previous studies of Houk and co-workers[37a] and Merry and Thomson.[37b]

A bond-stretching distortion that leaves the radical anion planar is also stabilizing but not as much as the bending type mode. On the other hand, the distortion to a perpendicular structure is actually destabilizing (last column Table VI) as reported by Houk and co-workers.[37a] Therefore, *internal rotation about the C–C bond will not be significant in the attack phase and will lag behind other distortions.* Likewise, *significant C–C stretching will be also inefficient as a "reactive distortion"*, since such stretching is quite expensive for the ground-state olefin and not too efficient in stabilizing the radical anion. On the other hand, the anti type bending distortion shown in **14** leads to maximal stabilization of the radical anion, and to minimal destabilization of the ground-state olefin. The bending mode (**14**) will thus be the prominent distortion in promoting the crossing in Figure 1.

The computational results follow the above predictions. All the transition states in Table III involve mainly an anti type bending with a small extent of C–C stretching (see **4** above). The internal C–C rotation lags behind even in the single-step reaction (reaction 7, Table III). Moreover, a small degree of internal C–C rotation appears in the reactions of those olefins whose radical anions themselves exhibit a small degree of such rotation (i.e., H₂C=CHF⁻, FHC=CHF⁻). The conclusion is clear-cut; the olefinic distortion reflects the type of avoided crossing in Figure 1. The extent of the distortion in the TS will reflect then the effort that is required in order *to shift a single electron from the nucleophile to the olefin.*

Three factors will determine the extent of TS distortions. The first factor is the electron-transfer energy gap, $I_{N:} - A_0^{\pi}$, in Figure 1. This is the gap that must be *overcome by distortions.* Therefore, everything else being equal, an increase in $I_{N:} - A_0^{\pi}$ will require a greater amount of distortion to reach the crossing point.

The second factor is the mode of delocalization of the odd electrons in π-CT (see **8A** and **8B**). An improper such delocalization (or an increase thereof) will reduce the steepness of descent of π-CT toward the crossing point. Therefore, a greater amount of distortions will be required to overcome a given gap and reach the crossing point.

The third factor is ΔE_{AT} (Figure 1). Generally, more exothermic ΔE_{AT} will require a lesser amount of distortions to reach the TS, provided that $I_{N:} - A_0^{\pi}$ and the delocalization factors remain approximately constant.

Since the same factors control also the height of the barrier, there should then exist a correlation between the TS distortions and the reaction barrier to attack, $E_{AT}^{\ddagger}$. The correlation is illustrated in Table VII, where the distortion efforts of the study reactions (1-8) are collected along with the corresponding barriers and reactivity factors. The distortion efforts are expressed as percentages of the entire distortion, from reactant to carbanionic product. The olefinic distortions that are considered are the CC stretching and the β,γ bending angles. Listed in addition are the H*–C bond orders and percentages of formation (H* = nucleophile).

There appears to exist a general correlation between the distortion effort (% CH*, % CC, % ($\beta + \gamma$)) and the barrier $E_{AT}^{\ddagger}$; the larger the barrier the larger (generally) the distortion effort. This correlation implies that the barrier indeed *drives primarily from the distortion effort* to reach the TS. A similar conclusion has been derived by Houk and co-workers[12a,b] using a Morokuma-type analysis.

Table VII demonstrates also the workings of the three geometry (and barrier) controlling factors. The importance of the delocalization factors (f') is reflected by comparing reactions 2 vs. 3 and 7 vs. 8. In both comparisons the increased distortion effort results from the delocalization modes of $(H_2C=CHX)^-$ (X = Cl, F), which favors reaction 2 over 3 and 8 over 7 (see eq 11 and 12). This *increased or improper* delocalization requires a larger distortion effort to achieve the TS, and in this respect, we are in complete agreement with Bernasconi.[5d]

The effect of increasing exothermicity (ΔE_{AT}) on TS geometry is reflected by, e.g., the smaller distortion efforts in reaction 6 vs. reaction 1, while the effect of decreasing the electron-transfer energy gap ($I_{N:} - A_0^{\pi}$) is projected by the smaller distortions of reaction 8 in comparison with reactions 6 and 4.

The crossing requirements of Figure 1 seem, therefore, to dominate the trends in the addition step. Thus, the olefin distorts and, *simultaneously*, the nucleophile approaches the center of attack: all these just in a measure so that, a single electron can shift from the nucleophile to the olefin and cause *synchronous* bond interchange (N:⁻ + C=C → N–C–C:⁻) As the electron-transfer energy gap ($I_{N:} - A_0^{\pi}$) decreases, at some limit, a mere olefinic distortion and/or solvent reorganization[14e,g,35] will suffice to lead to crossing (N:⁻/C=C → N·/(C=C⁻). A single electron transfer (SET) will then precede bond interchange and compete with the synchronous additions step of the NVS reaction.[38]

(37) (a) Paddon-Row, M. N.; Rondan, N. G.; Houk, K. N.; Jordan, K. D. *J. Am. Chem. Soc.* **1982**, *104*, 1143. (b) Merry, S.; Thomson, C. *Chem. Phys. Lett.* **1981**, *82*, 373.

(38) (a) SET in NVS type reactions is described for example in: Bunnett, J. F.; Creary, X.; Sundberg, J. E. *J. Org. Chem.* **1976**, *41*, 1701. (b) The feasibility of SET in NVS reactions has been considered before by: Truce, W. E.; Rossmann, M. G.; Perry, F. M.; Burnett, R. M.; Abraham, D. J. *Tetrahedron* **1965**, *21*, 2899. (c) See also ref 1a,b and 2b.

240

J. Am. Chem. Soc. **1986**, *108*, 240–244

The above discussion can be extended to the expulsion step whose TS geometries and barriers derive from the crossing requirements of Figure 2 (compare **6A** vs. **6B** above). A link can thus be drawn between barriers, TS geometries, and the distortion efforts required to shift a single electron in both the addition and elimination steps of NVS reactions.

Concluding Remarks

The state correlation diagram model[13,14] provides a methodology for piecing up a reaction profile from its component building blocks. For NVS reactions, the model is shown to lead to a unified understanding of the factors controlling the mechanistic choice of a given reactant pair (N:⁻/olefin), the variation of the reaction barriers, and the geometries of the transition state. The addition and elimination steps of NVS (eq 1) are shown to consist of trends that project the nature of these steps as processes that involve single electron shifts synchronized with bond interchange.

Supplementary Material Available: Four tables containing DZ//4-31G energies and geometries of olefins and A_1 and A_2 carbanions. Included also are outlines for calculating W_1 indices of radical anions, A_{CX} and $G(A_2^*)$ values (6 pages). Ordering information is given on any current masthead page.

Acceptor, Donor, and Captodative Stabilization in Transition States of 5-Hexen-1-yl Radical Cyclizations

Seung-Un Park, Sung-Kee Chung,*[1] and Martin Newcomb*[2]

Contribution from the Department of Chemistry, Texas A&M University, College Station, Texas 77843. Received May 17, 1985. Revised Manuscript Received October 7, 1985

Abstract: Rate constants and activation parameters for cyclization of the 6-substituted hex-5-en-1-yl radicals (6-cyano (**1b**), 6-methoxy (**1c**), and 6-cyano-6-methoxy (**1d**)) have been determined. At 50 °C, the rate constants for cyclization to the corresponding cyclopentylmethyl radicals are 1.65×10^8, 1.45×10^6, and 2.49×10^8 s⁻¹, respectively. The rate accelerations for the cyclizations of **1b–d** relative to that of the parent radical, hex-5-en-1-yl (**1a**), are discussed in terms of the substituents' perturbations of the highest occupied (HOMO) and lowest unoccupied molecular orbital (LUMO) of the alkene moiety. The large rate accelerations of **1b** and **1d** (275-fold and 415-fold, respectively, at 50 °C) result primarily from increased interaction of the semioccupied molecular orbital (SOMO) with the alkene LUMO, whereas the small rate acceleration of **1c** results from increased SOMO–HOMO interaction. Radicals **1b** and **1d** were found to have looser, hence earlier, transition states for cyclization than do **1a** and **1c**. Comparison of the E_a's for **1b–d** relative to that for **1a** indicates that there is a slight extra stabilization (captodative effect) in the transition state for cyclization of **1d**.

The cyclization of 5-hexen-1-yl radicals, especially that of the parent radical **1a**, have been studied in some detail. Radical **1a** cyclizes predominantly to cyclopentylmethyl (**2a**) with a rate constant of 2.5×10^5 s⁻¹ at 25 °C;[3] the regioselectivity results primarily from stereoelectronic effects favoring the transition state which leads to **2a** over that leading to the more thermodynamically stable radical, cyclohexyl.[4] The cyclizations of **1a** and its ana-

a, R = R' = H; b, R, R' = H, CN; c, R, R' = H, OCH_3; d, R, R' = CN, OCH_3

logues have been used extensively in mechanistic studies, both as qualitative probes to implicate free radicals as intermediates in reaction sequences and as quantitative "radical clocks",[4] and

recently there has been an increasing interest in synthetic applications of hexenyl-radical cyclizations.[5]

A variety of alkyl-substituted, bicyclic, and heteroatom-containing analogues of **1a** have been studied,[4] but little is known about the effects on cyclization of radical-stabilizing groups on the terminus of the alkene moiety in **1a**. This is unlike the case for intermolecular radical additions to substituted olefins where several systems have been studied, and the results have been collected in a succinct review by Giese.[6] In this paper, we report the effects on the cyclization rates of incorporating acceptor and donor groups at the incipient radical center in **1a** (radicals **1b–d**). Radicals are stabilized by acceptors and donors, and when both are present in the same system, increased stabilization over that of the sum of the individual components (known as captodative stabilization, mero stabilization, or push-pull stabilization) is

(1) Current address: Smith Kline & French, Philadelphia, PA 19101.
(2) Camille and Henry Dreyfus Teacher–Scholar, 1980–1985.
(3) Chatgilialoglu, C.; Ingold, K. U.; Scaiano, J. C. *J. Am. Chem. Soc.* **1981**, *103*, 7739–7742.
(4) (a) Beckwith, A. L. J.; Ingold, K. U. In "Rearrangements in Ground and Excited States"; Mayo, P. d. Ed.; Academic Press: New York, 1980; Vol. 1, Essay 4. (b) Surzur, J.-M. In "Reactive Intermediates", Abramovitch, R. A., Ed.; Plenum Press: New York, 1982; Vol. 2, Chapter 2. (c) Beckwith, A. L. J. *Tetrahedron* **1981**, *37*, 3073–3100.

(5) Many examples are given in ref 4. For recent representative examples, see: (a) Hart, D. J. *Science (Washington, D.C.)* **1984**, *223*, 883–887. (b) Curran, D. P.; Rakiewicz, D. M. *J. Am. Chem. Soc.* **1985**, *107*, 1448–1449. (c) Stork, G.; Kahn, M. *Ibid.* **1985**, *107*, 500–501. (d) Burnett, D. A.; Choi, J.-K.; Hart, D. J.; Tsai, Y.-M. *Ibid.* **1984**, *106*, 8201–8209. (e) Hart, D. J.; Tsai, Y.-M. *Ibid.* **1984**, *106*, 8209–8217. (f) Ladlow, M.; Pattenden, G. *Tetrahedron Lett.* **1984**, *25*, 4317–4320. (g) Clive, D. L. J.; Beaulieu, P. L.; Set, L. *J. Org. Chem.* **1984**, *49*, 1313–1314. (h) Nishiyama, H.; Kitajima, T.; Matsumoto, M.; Itoh, K. *Ibid.* **1984**, *49*, 2298–2300. (i) Beckwith, A. L. J.; O'Shea, D. M.; Roberts, D. H. *J. Chem. Soc., Chem. Commun.* **1983**, 1445–1446. (j) Ueno, Y.; Chino, K.; Watanabe, M.; Moriya, O.; Okawara, M. *J. Am. Chem. Soc.* **1982**, *104*, 5564–5566.
(6) Giese, B. *Angew. Chem., Int. Ed. Engl.* **1983**, *22*, 753–764.